[redacted]

DEPARTMENT OF THE NAVY

DAVID TAYLOR MODEL BASIN
WASHINGTON, D.C.

HYDROMECHANICS

O

AERODYNAMICS

O

STRUCTURAL MECHANICS

O

APPLIED MATHEMATICS

O

ACOUSTICS AND VIBRATION

PRESSURE DISTRIBUTION ON TOWED AND PROPELLED STREAMLINE BODIES OF REVOLUTION AT DEEP SUBMERGENCE

by

John L. Beveridge

Distribution of this document is unlimited.

HYDROMECHANICS LABORATORY
RESEARCH AND DEVELOPMENT REPORT

June 1966

Report 1665

DAVID TAYLOR MODEL BASIN
WASHINGTON, D. C. 20007

PRESSURE DISTRIBUTION ON TOWED AND PROPELLED STREAMLINE BODIES OF REVOLUTION AT DEEP SUBMERGENCE

by

John L. Beveridge

June 1966

Report 1665
S-R009 01 01

TABLE OF CONTENTS

LIST OF FIGURES

LIST OF TABLES

NOTATION

A	Propeller disk area
a^*	Displacement thickness in boundary layer for axisymmetric flow
C_T	Propeller thrust-loading coefficient, $\frac{T}{\frac{1}{2}\rho A V_a^2}$
D	Maximum diameter of a body of revolution
d	Propeller diameter
J_a	Propeller apparent speed coefficient, $\frac{V_0}{nd}$
K_T	Propeller thrust coefficient, $\frac{T}{\rho n^2 d^4}$
L	Length of a body of revolution
M	Nondimensional source or sink strength, $\frac{m}{V_0 L^2}$
m	Dimensional source or sink strength
n	Frequency of propeller revolution
$\vec{n}$	Unit vector in normal direction
P	Pressure, or a general point
P_i	Control point
Q	Point source output
q	Surface source output
q_0	Stagnation pressure, $\frac{1}{2}\rho V_0^2$
R	Radius vector
R_0	Propeller radius

r	Cylindrical coordinate or offset to a meridian profile
r^*	Radius to equivalent body with added displacement thickness
r'	Nondimensional radius vector, $\frac{R}{L}$
S	Surface area
T	Propeller thrust
V	Total fluid velocity
V_a	Propeller speed of advance
V_n	Normal velocity or induced normal velocity
V_0	Undisturbed fluid velocity
V_q	Resultant induced velocity
V_r	Radial induced velocity
V_T	Tangential induced velocity
V_x	Axial induced velocity
v_b	Nondimensional tangential velocity $\frac{V_{Tb}}{V_0}$ along body surface without propeller
v_n	Nondimensional velocity, $\frac{V_n}{V_0}$
v_q	Nondimensional velocity, $\frac{V_q}{V_0}$
v_r	Nondimensional velocity, $\frac{V_r}{V_0}$
v_T	Nondimensional velocity, $\frac{V_T}{V_0}$
v_x	Nondimensional velocity, $\frac{V_x}{V_0}$

W_0	Effective wake fraction, $\left(1 - \frac{V_a}{V_0}\right)$
X, Y	Dimensional rectangular coordinates
x, y	Nondimensional rectangular coordinates $\frac{X}{L}$ and $\frac{Y}{L}$
α	Angle of inclination to body surface
β	Angle between axis of body and r' for discrete M_j's
$\vec{\nabla}$	Vector operator del
θ	Angle between resultant and x-component of propeller induced velocity
Λ^*	Displacement area
ν	Kinematic viscosity
ρ	Mass density
ϕ	Total velocity potential
ϕ_1	Velocity potential for body
ϕ_2	Velocity potential for propeller
ϕ_3	Additional velocity potential for propeller interference

Subscripts: i, j Matrix position.

ABSTRACT

Measured and computed pressure distributions were obtained for a well-streamlined body of revolution (fineness ratio of ten to one), with and without a propeller, at deep submergence. Velocity distributions over the surface of the body with and without an added boundary-layer displacement-thickness are obtained from the velocity-potential function for a surface distribution of sources. Propeller-induced velocities in the near field ahead of a propeller are estimated from a uniform sink-disk representation and a single sink representation is used for large distances from the propeller. Propeller interference (image) effects are obtained from discrete singularities placed along the body axis. Within the field of propeller influence, differences occur in the theoretical and experimental pressure distributions. These discrepancies are discussed.

INTRODUCTION

Studies of pressure distributions for ships, submarines, and torpedoes have used, as a point of departure, information obtained from more basic work with bodies of revolution. This report deals with the problem of pressure distributions on the surface of submerged streamline bodies of revolution with and without a stern propeller.* Specifically, the problem is to develop an analytic method, based on existing theory, that will permit predictions of pressure distributions with acceptable accuracy. Such pressure distributions can be used to obtain detailed information on the distribution of interaction forces (e.g., along the afterbody) as contrasted to methods which give only total forces. With regard to these propeller-body interaction forces, gross effects may be determined by means of Lagally's theorem.[1, 2, 3]

Some recent contributors to the subject of pressure distributions for towed and propelled bodies of revolution are Amtsberg,[4] Dreger,[5] Korvin-Kroukovsky,[6] and the author.[7] Amtsberg reported propulsion interaction experiments on "so-called" substitute bodies of revolution (i.e., bodies of revolution whose sectional-area curves represent ship-shaped forms). These experiments included measurements of the pressure distribution along the lower meridian of two such forms. Dreger confined his efforts to the mathematical computation of pressure distributions and thrust deduction in potential flow. Korvin-Kroukovsky presented pressure measurements obtained in a wind tunnel as well as computed pressure distributions for a model of U. S. Airship AKRON.

---

*The present investigation was supported by the Bureau of Ships Fundamental Hydromechanics Research Program.

[1]References are listed on page 21.

Since the advent of ALBACORE, having a fineness ratio of 7.3, the trend in single-screw submarine design, has been to higher fineness ratios (for reasons other than hydrodynamic) and, as a result, pressure and velocity information on bodies of revolution of about ten to one are needed. The investigations cited above did not consider bodies of revolution whose shape and fineness ratio are representative of current submarine designs; therefore, computations and experiments were performed with a TMB Series 58 form[8] having a ten to one fineness ratio. In the present study the usual computational procedure of considering propeller and body flow-fields separately and combining them later is followed. The extent of the work includes not only the presentation of a general computational method, but makes available new experimental pressure-distribution data, for a body of high fineness ratio, to which other analytical methods can be compared.

The principal *assumptions* and *limitations* that are involved in the computational method are summarized as follows:

1. It is assumed that the fluid is incompressible and inviscid. However, calculations were performed for both a bare body and an equivalent body with the displacement thickness of the boundary layer considered as part of the body.

2. It is assumed that the induced steady-state velocity field immediately ahead of a propeller can be estimated from the velocity induced by a uniform distribution of sinks on a circular disk, and that a single sink is adequate for estimating propeller-induced velocity at distances greater than one propeller diameter from the propeller plane.

3. Propeller interference effects are considered by introducing discrete singularities along the axis of the body. The boundary condition that the velocity normal to the body surface must be zero is satisfied only at certain control points located on the afterbody. Since the body is smooth and the propeller interference velocities are small, it is assumed that the discrete distribution is a good approximation to a continuous distribution.

INDUCED VELOCITY FIELD OF PROPELLER

If the propeller is replaced by a sink disk, its steady-state velocity field may be computed by using the method of Küchemann and Weber.[9] As a further simplification it will be shown that a single sink representation of the propeller is adequate, compared to a sink disk, for computing induced velocities at distances greater than one diameter forward of a propeller. These mathematical propeller models give the propeller-induced velocity field as a function of propeller thrust loading, but do not consider propeller blade thickness. The assumption of no thickness effect may not be adequate. If the propeller is replaced by a sink located at the propeller center, the velocity induced at a point P is as shown in Figure 1.

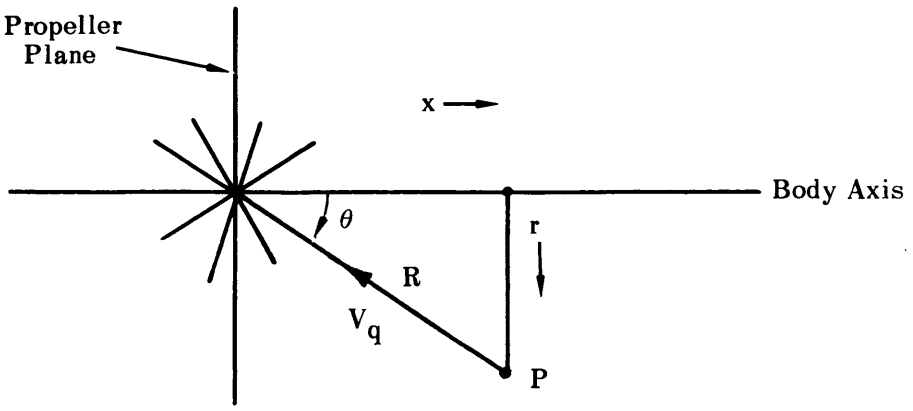

Figure 1 – Flow Due to a Three-Dimensional Sink

A three-dimensional sink has the velocity potential

$$\phi_2 = -\frac{M.}{R} \qquad [1]$$

Differentiate ϕ_2 with respect to R to obtain

$$V_q = -\frac{\partial \phi_2}{\partial R} = -\frac{M}{R^2} \qquad [2]$$

where $m = \frac{Q}{4\pi}$ is the strength of a point sink, Q being the volume rate of flow into the sink,

R is the distance from the sink to a field point P, and

V_q is the induced velocity.

By substituting $\frac{Aq}{4\pi}$ for m in Equation [2], a convenient nondimensional form is obtained:

$$\frac{V_q}{q} = -1/4\left(\frac{R_0}{R}\right)^2 \qquad [3]$$

where A is the propeller disk-area,

R_0 is the propeller radius, and

q is the surface sink input.

Nondimensionalizing the coordinates $P(X, r)$ in Figure 1, with respect to propeller radius, and using Equation [3], the X and r components of velocity V_q are

$$\frac{V_x}{q} = -\frac{1}{4}\left[\frac{1}{\left(\frac{X}{R_0}\right)^2 + \left(\frac{r}{R_0}\right)^2}\right] \cos\theta \qquad [4a]$$

and

$$\frac{V_r}{q} = -\frac{1}{4}\left[\frac{1}{\left(\frac{X}{R_0}\right)^2 + \left(\frac{r}{R_0}\right)^2}\right] \sin\theta \qquad [4b]$$

Comparative data for the induced velocities from a uniform distribution of sinks on a circular disk,[9] and the induced velocities calculated from Equations [4a] and [4b] are tabulated in Table 1 for various values of the cylindrical coordinate $\frac{r}{R_0}$ for a constant value of $\frac{X}{R_0} = 2.0$. The propeller was represented by a sink disk for $\frac{X}{R_0} < 2$ and a single sink for $\frac{X}{R_0} > 2$. Since V_x and V_r are themselves small fractions of q and the undisturbed velocity V_0, it is believed that a single sink should give sufficiently accurate values of propeller-induced velocities for estimating pressure distributions at $\frac{X}{R_0} > 2$.

FLOW ABOUT BODIES OF REVOLUTION

FLOW WITHOUT PROPELLER

A solution for the potential flow about a body leads to a solution of the Laplace equation $\vec{\nabla}^2\phi = 0$ subject to certain boundary conditions. Methods of solving the direct problem of

determining the flow about a prescribed axisymmetric body have been investigated by Kaplan,[10] Young and Owen,[11] Vandrey,[12] Landweber,[13] and Smith and Pierce.[14] In the following, then, only a brief summay of the method used will be presented.

TABLE 1

Comparison of Propeller Induced Velocities from a Single Sink and a Uniform Sink Distribution

$\left(\frac{X}{R_0} = 2\right)$

$\frac{r}{R_0}$	$\left\lvert\frac{V_x}{q}\right\rvert$		$\left\lvert\frac{V_r}{q}\right\rvert$	
	Sinks Uniformly Distributed on a Circular Disk*	Single Sink	Sinks Uniformly Distributed on a Circular Disk*	Single Sink
0.0	0.0525	0.0625	0.0000	0.0000
0.2	0.0525	0.0616	0.0048	0.0061
0.4	0.0509	0.0589	0.0088	0.0118
0.6	0.0477	0.0549	0.0119	0.0165
0.8	0.0446	0.0500	0.0151	0.0200
1.0	0.0414	0.0447	0.0183	0.0224
1.2	0.0382	0.0394	0.0199	0.0236
1.4	0.0334	0.0344	0.0207	0.0241
1.6	0.0302	0.0298	0.0207	0.0238
1.8	0.0255	0.0256	0.0207	0.0231
2.0	0.0223	0.0221	0.0207	0.0221

*From Reference 9.

The potential due to a surface distribution of sources m is

$$-\int_S \frac{m\,ds}{R} \qquad [5]$$

and for a prescribed body, the source strengths are calculated for the condition of no flow through the body surface, i.e., $V_n = 0$. The unknown source strengths can be obtained by solving a Fredholm integral equation of the second kind. Smith and Pierce[14] programmed a solution on the IBM-704 for this integral equation by using a set of linear algebraic equations.

It has been reported[16] that consideration of the influence of the boundary layer usually leads to an improvement in the accuracy of estimating actual pressure distributions over the distributions obtained for bodies of revolution in a potential flow. In accounting for the difference between actual pressure and potential pressure which exists, particularly in the region of the rear stagnation point, the so-called displacement thickness of the boundary layer is considered as part of the body. By repeating the potential flow calculation for an equivalent body whose ordinates include this added thickness, closer agreement with the actual pressure distributions might be expected because of the more realistic shape of the bounding streamlines.

Granville[15, 16] has reviewed the subject of turbulent boundary layers in a pressure gradient and presented a method for calculating their most important characteristics. A radius r^* to the surface of an equivalent body of revolution is defined[16] by

$$r^* = r_w + a^* \cos \alpha = \sqrt{r_w^2 + 2 \Lambda^* \cos \alpha}$$

where r_w is the radius of a body of revolution,

a^* is the displacement thickness of the boundary layer normal to the surface of an axisymmetric body,

Λ^* is the displacement area, and

α is the angle of inclination of the body surface to the body axis.

Table 2 gives the velocity distribution in a potential flow as obtained from the IBM-704 program[14] for TMB Model 4198 with and without an added displacement thickness. In Figure 2 the nondimensional offsets y for the bare body and $\frac{r^*}{L}$ for the equivalent body of revolution are plotted versus length fraction x (based on true body length). Attention is called to the fact that a tail extending to infinity was added to account for the displacement thickness of the boundary layer in the case of the equivalent body. As anticipated, the data in Table 2 reveal little difference between the two velocity distributions except in the vicinity of the stern ($x = 1.0$) where the velocity distribution for the equivalent body approximates more closely conditions in a real viscous flow.

COMBINED FLOW DUE TO BODY AND PROPELLER

A meridian profile may be defined in cylindrical coordinates as shown in Figure 3. In Figure 3 all lengths are expressed nondimensionally as fractions of the body length L, and all velocities are expressed as fractions of the transport velocity V_0. For convenience in this part of the problem the origin is taken at the tail of the body.

TABLE 2

Velocity Distribution in a Potential Flow

Length Fraction x		Velocity Ratio, v_b	
		Model 4198	Equivalent Body
	0.030	0.968	0.973
	0.060	0.997	0.994
	0.085	1.0075	1.004
	0.175	1.024	1.022
	0.275	1.030	1.027
	0.375	1.027	1.025
	0.525	1.020	1.020
Control Points	0.725	1.010	1.009
	0.825	0.995	0.996
	0.875	0.983	0.986
	0.925	0.965	0.972
	0.950	0.952	0.971
	1.000	0.000	0.970
	1.030	----	0.973

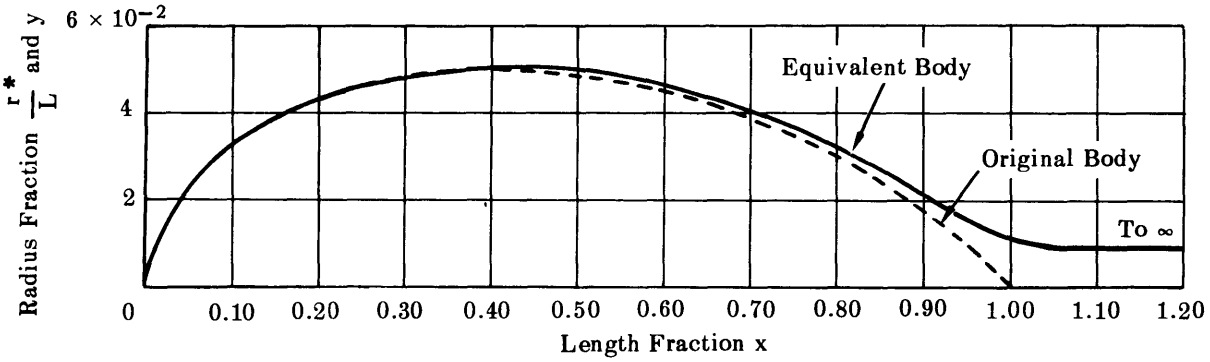

Figure 2 – Half Profile of Equivalent and Original Body of Revolution

Since the total velocity is the gradient of the total potential, the velocity formulation is accomplished by summing the contributions of all pertinent potentials,

$$\phi = \phi_1 + \phi_2 + \phi_3 \qquad [6]$$

and

$$-\vec{V} = \vec{\nabla}\,\phi_1 + \vec{\nabla}\,\phi_2 + \vec{\nabla}\,\phi_3 \qquad [6a]$$

where ϕ is the total velocity potential,

ϕ_1 is the velocity potential for the body in uniform flow,

ϕ_2 is the velocity potential for the propeller, and

ϕ_3 is the interference velocity potential required to satisfy boundary conditions on the body.

When the total velocity is obtained from Equation [6a] the pressure distribution is appropriately calculated for points on the body from the Bernoulli equation.

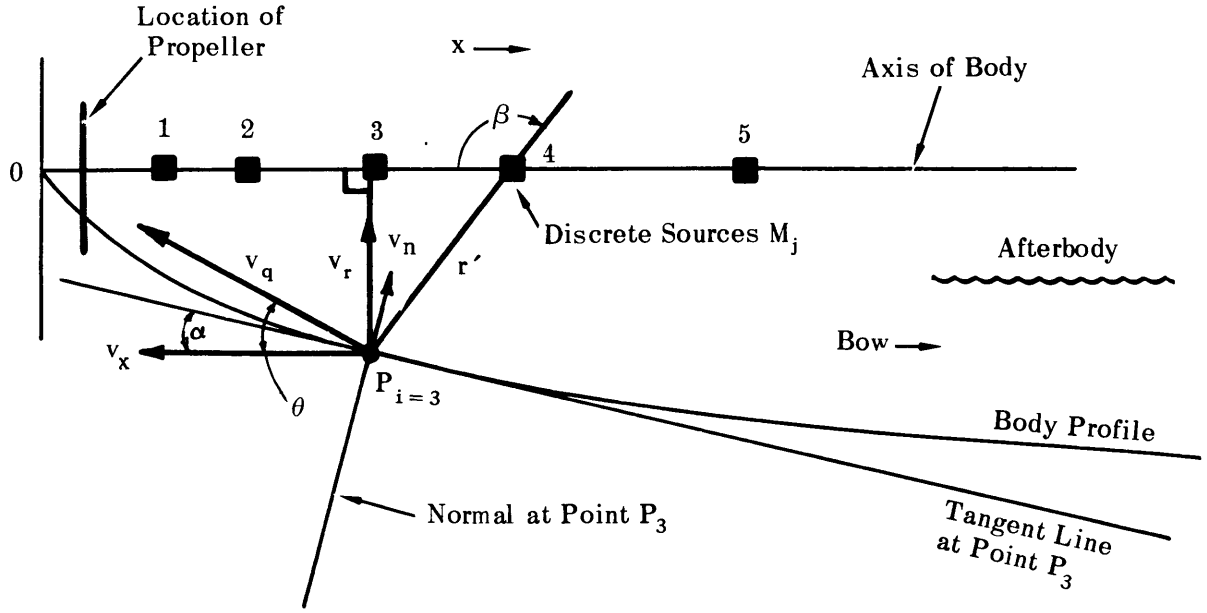

Figure 3 – Meridian Profile of a Body of Revolution Depicting Velocities Induced by a Stern Propeller

The mathematical model of a stern propeller will induce velocities along the afterbody that are normal to the body surface. These normal velocities must be balanced by equal and opposite velocities to satisfy the boundary condition $\vec{\nabla}\phi \cdot \vec{n} = 0$ where $\vec{n}$ is the unit vector in the normal direction. To balance the normal velocity induced by the propeller at the body surface, a set of five discrete sources M_j are arranged on the axis of the body. At each control point $P_i\ (x_i, r_i)$ (see Figure 3) the sum of the outward directed normal velocities due to all discrete sources must be equal to and opposite to the normal velocity induced by the propeller. At point $P_i\ (x_i, r_i)$, the propeller induced normal velocity is

$$v_{q_i} \sin(\theta_i - \alpha_i) = v_{n_i}$$

and v_{n_i} balanced by the contribution of the discrete M_j's gives

$$v_{n_i} + \sum_{j=1}^{5} \frac{M_j \sin(\beta_{ji} - \alpha_i)}{(r'_{ji})^2} = 0 \qquad [7]$$

where v_{n_i} is the nondimensional propeller induced normal velocity $\frac{V_{n_i}}{V_0}$,

M_j is the nondimensional source strength $\frac{m_j}{V_0 L^2}$,

β_{ji} is the angle between axis of body and r'_{ji} for discrete sources,

α_i is the angle between the tangent to the body surface and the body axis,

θ_i is the angle between resultant and x-component of propeller induced velocity, and

r'_{ji} is the nondimensional radius vector.

Equation [7] results in a system of five linear nonhomogenous algebraic equations from which the unknown strengths M_j of the control sources may be solved.

When the unknown source strengths M_j are determined, the various contributions to the total velocity are summed according to Equation [6a]. The total tangential velocity at a point P_i on the body is, nondimensionally,

$$v_{T_i} = v_{b_i} + v_{q_i} \cos(\theta_i - \alpha_i) + \sum_{j=1}^{5} \frac{M_j \cos(\beta_{ji} - \alpha_i)}{(r'_{ji})^2} \qquad [8]$$

where the first term on the right side is the contribution due to the body without propeller, the second term is the contribution due to the propeller, and the third term is the contribution due to discrete sources (propeller image system). In regard to Model 4198, the third term was calculated only for the bare body and its values were assumed to be the same for the equivalent body. No iterations were performed to consider the interference effect of the discrete sources on the propeller model because for the present case the source strengths M_j were found to be very weak (Appendix A). Using the total tangential velocity obtained from Equation [8], the pressure coefficient is obtained from Bernoulli's equation, and is given by

$$\frac{P}{q_0} = 1 - v_T^2 \qquad [9]$$

where q_0 is the stagnation pressure $\frac{1}{2}\rho V_0^2$.

DISCUSSION OF MEASURED PRESSURES AND COMPUTED RESULTS

A description of the model and test procedure is contained in Appendix B. In Figure 4 the experimental and computed pressure distributions for Model 4198 are presented nondimensionally as curves of the pressure coefficient $\frac{P}{q_0}$, which is given by Equation [9]. It is seen that the influence of the propeller is not felt forward of station $x = 0.80$ for the given advance coefficient $J_a = 0.72$. At this advance coefficient the propeller thrust-loading coefficient C_T is 1.411, which represents the highest propeller load for which computations were made. These propeller coefficients are defined as $J_a = \frac{V_0}{nd}$ and $C_T = \frac{T}{\frac{1}{2}\rho A V_a^2}$

where T is propeller thrust,

n is frequency of propeller revolutions,

ρ is mass density,

A is propeller disk area,

d is propeller diameter,

V_0 is body speed, and

V_a is propeller speed of advance.

The salient features of the pressure distributions for both the towed and propelled conditions are confined to the last 20 percent of the body length. First, examine the *experimental results*. For the towed condition, without propeller, the pressure coefficient is positive aft of station $x = 0.80$ and continues upward in the same manner as would be expected in a frictionless flow except in the region very near the stern ending where it is seen to level off. At the stern a pressure coefficient of about 0.10 was measured whereas in a frictionless flow, a value of unity would occur. Turning now to the propelled condition, we see that the measured pressure coefficient rises slightly above zero aft of station $x = 0.80$, and then turns downward towards a negative value. All of the measured pressure data for the propelled conditions are

summarized in Figure 5 where the pressure coefficients $\frac{P}{q_0}$ measured at a number of body locations are plotted as a function of the propeller advance coefficient J_a. As would be expected, at stations close to the propeller the pressure coefficient is quite sensitive to propeller load.

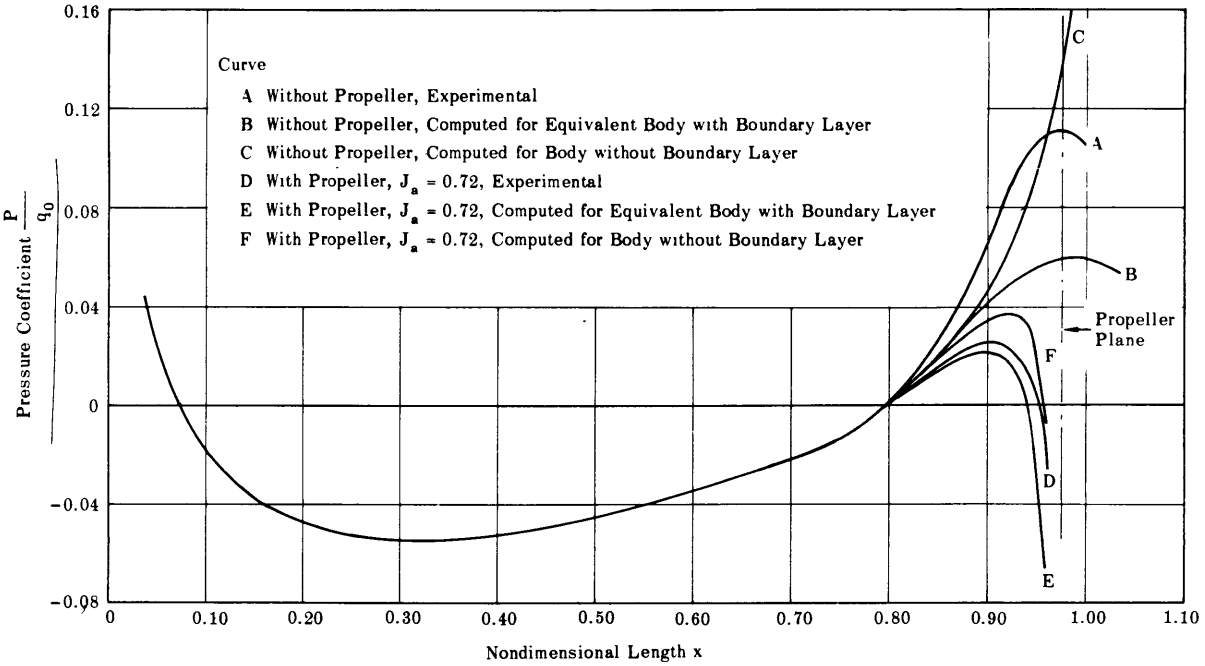

Figure 4 – Pressure Distribution along a Meridian for TMB Model 4198

Pressure distributions were computed from Equation [9] where the velocity v_T was calculated from Equation [8]. These computed results are presented in Figures 4 and 5 for comparison with the experimental results. We see from Figure 4 that the calculated equivalent body and experimental results for the towed condition agree very well over practically the entire body except for about the last 10 percent of the body length. In this region, the computed pressures for an equivalent body are somewhat lower than the test results. In the narrow range from $x \approx 0.90$ to the propeller plane, neither computed pressure distribution is in good agreement with the test curve. Of course, stagnation pressure occurs at the true stern ending if the boundary layer is not considered in performing the computation. Comparing the experimental and computed results in Figure 4 for the most heavily loaded propulsion condition ($J_a = 0.72$), we see that the experimental and theoretical pressure curves converge to the values obtained without a propeller at about $x = 0.80$. In the region between station $x = 0.80$ and the propeller plane the pressure computed for the equivalent body is a little lower than the test results, whereas for the bare body the pressure is a little higher. Included in Figure 5 is the calculated equivalent body variation of the pressure coefficient at station $x = 0.92$

as a function of propeller advance coefficient. At this location, the agreement with the experimental curve is good. In order not to clutter Figure 5, the remaining computed pressure curves for the propelled condition are shown in Figure 6.

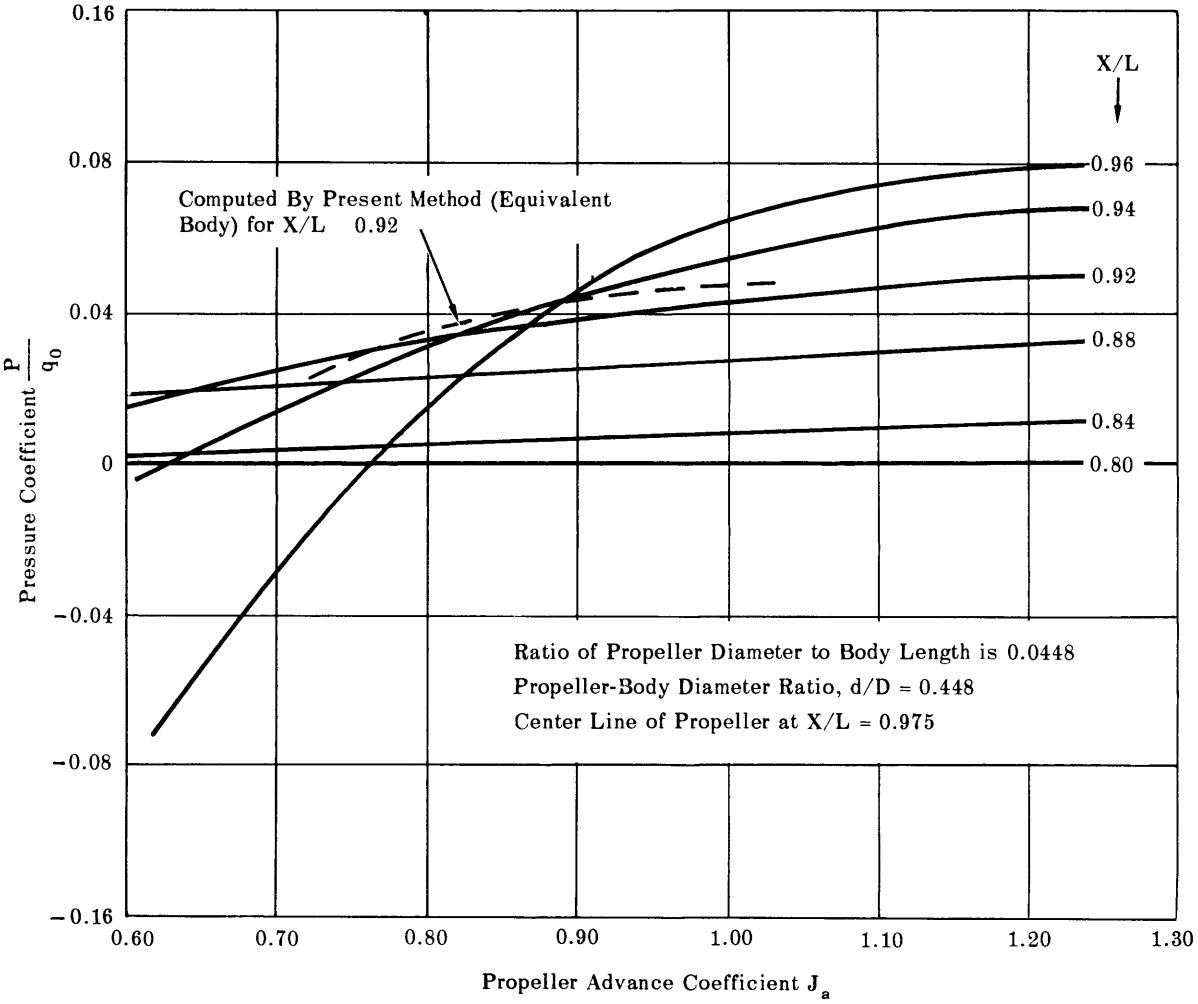

Figure 5 – Cross Plot of Pressure Coefficient versus Propeller Advance Coefficient as Obtained from Tests with TMB Model 4198 and Propeller 2861A

The pressure data presented may be used to compute thrust deduction. In particular, the resistance augmentation or thrust-deduction force may be obtained by summing over the body surface the axial forces associated with the pressure defect between the towed and propelled conditions. Compared to direct force measurements, integration of the pressure defect from the three sets of pressure curves shown in Figure 4 give the following results:

Condition	Thrust Deduction Coefficient, t		
	Pressure t_p	Frictional* t_f	Total t
Propulsion Test (direct force measurement)			0.090
Experimental Pressure	0.075	0.015	0.090
Computed Pressure (equivalent body)	0.041	0.015	0.056
Computed Pressure (bare body)	0.031	0.015	0.046

*The frictional thrust deduction coefficient t_f was assumed to be equal to the difference (0.015) between total t from the direct force measurements and t_p as obtained from the experimental pressure data. Other investigators have indicated about this same order of magnitude for the contribution of the shearing force to the total thrust deduction.

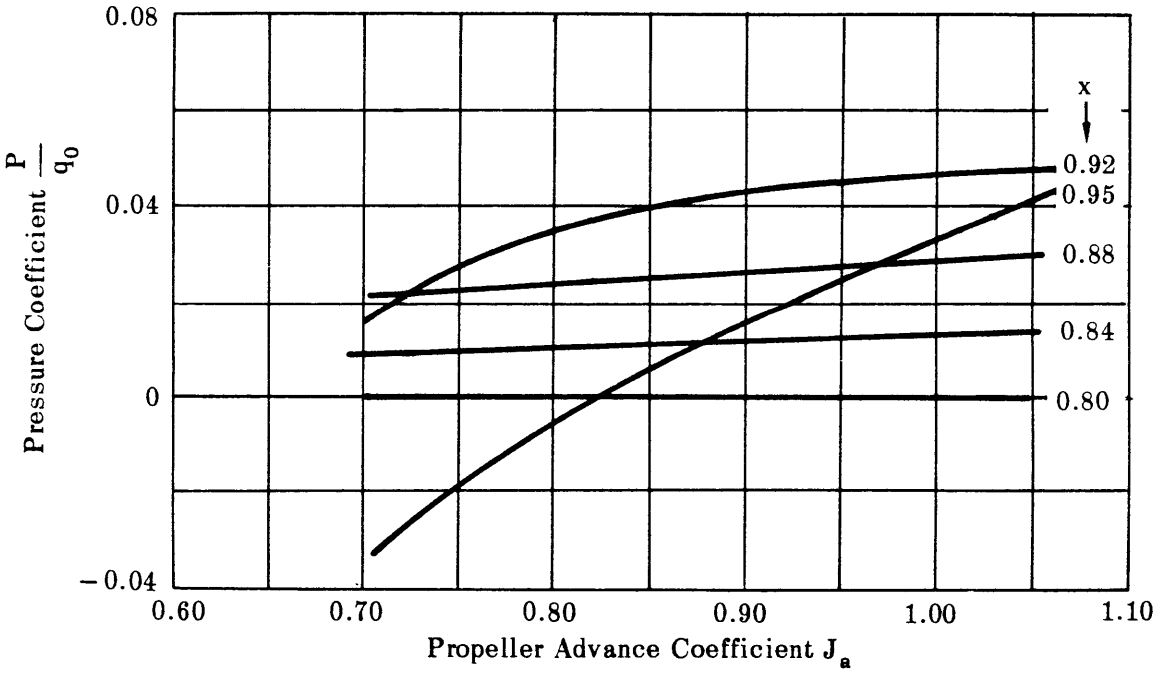

Figure 6 – Cross Plot of Pressure Coefficient versus Propeller Advance Coefficient as Computed for TMB Model 4198 and Propeller 2861A

As is seen from the tabulation, the integrated experimental pressure defect gives a reasonable value of 0.075 for t_p while the computed results are about 3 to 4 points too low. Only a marginal improvement in estimating thrust deduction is obtained for the equivalent body compared to the result for the bare body. The limits of integration used in computing t_p were from $x = 0.80$ to $x = 0.96$. It was not possible to obtain pressure measurements farther aft for the experiments with the propeller in place. Since the slopes of the sectional-area curve are small from station $x = 0.96$ to the propeller disk at $x = 0.975$, only slightly lower values for t_p result compared to those that would be obtained by extending the upper limit to the propeller disk.

To complete the analysis of the results shown in Figure 4, the following explanations are given for the relative positions of the three pressure distributions without propeller. In the region somewhat ahead of the stern ending ($X/L = 1$) the measured real viscous P/q_0 is higher than that computed for pure potential flow. This result has been observed by others[6,17,18] and could be related to the point of turbulent-flow separation at the stern.

Compared to the P/q_0 curve obtained by experiment without propeller, the results for the equivalent body are too low due to deficiencies in the equivalent body concept and in the method of calculation involving the theory of boundary layers in a longitudinal pressure gradient. With reference to the computed pressure distribution of the equivalent body for the propulsion condition, it leads to an under estimate of the pressure defect. Thus, the adequacy of the mathematical representation of the propeller (for determining induced velocities at points close to the propeller) in the present case may be questionable despite the fair agreement of the absolute pressure distribution as calculated and measured.

CONCLUSIONS

The principal findings which have resulted from this study are:

1. For the body and propeller configuration considered, propeller interference (image) effects were small (e.g., maximum discrete source strength was three percent of the singularity strength of the propeller).

2. Considering the displacement thickness of the boundary layer led to a more realistic computed pressure coefficient at the *stern ending*; however, it does not seem that this consideration gives an overall improvement in the present analytical results.

3. Propeller influence on the body pressure distribution was confined to the last twenty percent of the body length.

4. Integration of the experimental pressure curves produced a thrust-deduction coefficient that agreed with direct force measurements. A similar comparison using computed pressure curves resulted in thrust-deduction coefficients that were three to four points lower than that measured.

5. On the basis of the comparison between experimental and computed pressures the uniform sink disk representation of a propeller and the equivalent body concept are open to serious question. Further analytical study of the concepts and methods of computation presented here is definitely necessary.

APPENDIX A

DETAILS OF COMPUTATIONS

In connection with the pressure distributions computed for Model 4198, the following computational details for Equations [7] and [8] are presented.

1. *Contribution due to propeller* – In the section INDUCED VELOCITY FIELD OF A PROPELLER, propeller-induced velocities were nondimensionalized for comparative purposes, in terms of the induced velocity at the propeller disk itself. Since only the front part of the propeller acts like a sink, the actual sink strength density must correspond to the ultimate slipstream velocity. For use in Equations [7] and [8], we convert these velocities in terms of the undisturbed velocity V_0 as follows:[6, 7]

$$v_q = \frac{V_q}{q} \cdot \frac{q}{V_0}$$

with

$$\frac{q}{V_0} = (1 - w_0)\,[-1 + (1 + C_T)^{1/2}]$$

where V_q is the propeller resultant induced velocity,

q is the total surface sink input,

w_0 is the effective wake fraction, and

C_T is the propeller thrust-loading coefficient.

Three values of the conversion factor q/V_0 were calculated using the experimental data obtained at the following self-propulsion conditions:

J_a	$(1-w_0)$	C_T
0.722	0.74	1.411
0.818	0.74	0.904
1.031	0.74	0.267

2. *Contribution due to discrete sources* – In Figure 3 the five control points for the discrete sources M_j were chosen at fractions of body length x (measured from the propeller plane) as follows:

j	x	y	Cos α
1	0.050	0.015370	0.99717
2	0.075	0.018300	0.99470
3	0.125	0.024150	0.99325
4	0.175	0.029655	0.99320
5	0.275	0.038605	0.99560

where y is the offset to a meridian profile and α is the angle between the tangent to the body surface and the body axis. For the specific example of Model 4198, the matrix equations resulting from Equation [7] for the unknown source strengths M_j are

$$v_{n1} + 4218.6228\,M_1 + 698.3240\,M_2 + 49.7703\,M_3 + 13.5278\,M_4 + 3.1807\,M_5 = 0$$

$$v_{n2} + 572.0963\,M_1 + 2964.7492\,M_2 + 158.9848\,M_3 + 28.3864\,M_4 + 5.1208\,M_5 = 0$$

$$v_{n3} + 31.2601\,M_1 + 106.2433\,M_2 + 1703.6912\,M_3 + 173.9916\,M_4 + 11.8030\,M_5 = 0$$

$$v_{n4} + 7.8563\,M_1 + 16.9403\,M_2 + 123.9944\,M_3 + 1131.6302\,M_4 + 35.0577\,M_5 = 0$$

$$v_{n5} + 1.8125\,M_1 + 2.7786\,M_2 + 7.3243\,M_3 + 25.1696\,M_4 + 669.2430\,M_5 = 0$$

where the normal velocity v_n induced by the propeller is tabulated below for the three propeller advance coefficients previously mentioned.

Propeller Induced Velocity v_n
(Inwardly Directed)

i \ J_a	0.722	0.818	1.031
1	−0.014174	−0.009743	−0.003221
2	−0.004216	−0.002898	−0.000958
3	−0.000879	−0.000604	−0.000200
4	−0.001012	-0.000696	−0.000230
5	−0.000135	−0.000093	−0.000031

Computed source strengths M_j for the most heavily loaded propeller condition (J_a = 0.722, C_T = 1.411) are:

$$M_1 = 32.25139 \times 10^{-7}$$

$$M_2 = 7.74224 \times 10^{-7}$$

$$M_3 = 3.23658 \times 10^{-7}$$

$$M_4 = 8.20027 \times 10^{-7}$$

$$M_5 = 1.55389 \times 10^{-7}$$

These results show that in moving away from the propeller (from $x = 0.05$ to $x = 0.275$) the source strength required to satisfy the boundary condition at the body surface, in the presence of the propeller, is reduced approximately by a factor of 20. A comparison of the propeller source strength M_{prop} at maximum load to the maximum discrete source strength M_1 reveals $\frac{M_1}{M_{prop}} = 0.032$.

APPENDIX B

DESCRIPTION OF MODEL AND TEST PROCEDURE

A 15-foot body of revolution (TMB Model 4198) representing a Series 58 form with a ten to one fineness ratio was used for the experiments and computable example. This model is a well-streamlined form with maximum section located at station $x = 0.40$, a prismatic coefficient of 0.60, and zero tail radius. Table 3 gives the offsets and other geometric particulars for Model 4198. A photograph of Model 4198 is shown in Figure 7. Piezometer taps were located along the lower meridian at the following fractions of model length: $x = 0.25$, 0.30 0.35, 0.40, 0.45, 0.50, 0.60, 0.70, 0.80, 0.85, 0.90, 0.92, 0.94, 0.95, 0.965, and additionally, for tests without propeller, at 0.975, 0.98, and 1.00. Propeller 2861, a 4-bladed TMB stock propeller with $d/L = 0.0448$, was located at station $x = 0.975$ for the propulsion tests.

Tests were conducted at approximately a 10-foot depth of submergence measured to the body axis. At this submergence there were no calculated free-surface effects. Towing was accomplished with a single strut whose towpoint was about 30 percent of the body length aft of the bow. The arrangement of the propeller motor and ballast within the model was that used for most routine submerged propulsion tests conducted at the Model Basin.[7] All tests were carried out at a 10-knot carriage speed.

A number of U-tube manometer boards were mounted on the towing carriage. Each U-tube was partially filled with carbon tetrachloride containing a small amount of dye. One leg was connected to a piezometer tap and the other leg was connected to a water-filled reference tank at atmospheric pressure. With water over the carbon tetrachloride on both sides of the U-tube a more sensitive measure of differential head was obtained. Pressure measurements were carried out in the following manner: Zero readings were obtained for each tube; then, from a series of constant speed runs the equilibrium run was determined by observing the maximum differential head. Normally, about five runs were necessary to reach equilibrium for the 10-knot carriage speed.

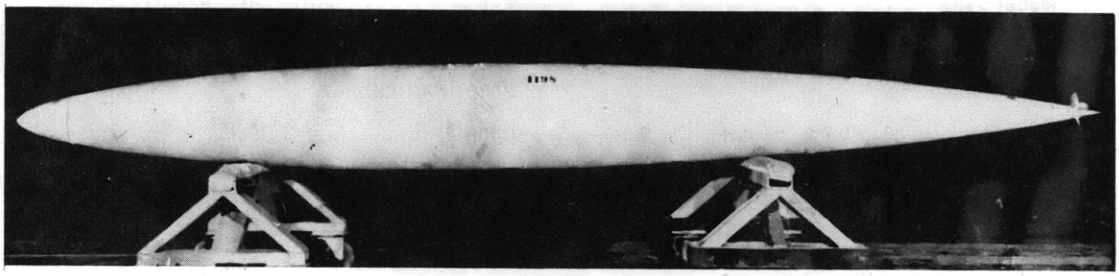

Figure 7 – Series 58 Form, TMB Model 4198

TABLE 3

Offsets and Particulars for Series 58 Form, Model 4198

The present method of defining bodies of revolution is given in Reference 8.

x	X in.	$\frac{Y}{D}$	Y in.	x	X in.	$\frac{Y}{D}$	Y in.
0.00	000.0	0.0000	0.000	0.52	93.6	0.4818	8.672
0.02	3.6	0.1427	2.569	0.54	97.2	0.4755	8.559
0.04	7.2	0.2029	3.652	0.56	100.8	0.4684	8.431
0.06	10.8	0.2490	4.482	0.58	104.4	0.4603	8.285
0.08	14.4	0.2873	5.171	0.60	108.0	0.4513	8.123
0.10	18.0	0.3200	5.760	0.62	111.6	0.4414	7.945
0.12	21.6	0.3485	6.273	0.64	115.2	0.4305	7.749
0.14	25.2	0.3734	6.721	0.66	118.8	0.4187	7.537
0.16	28.8	0.3953	7.115	0.68	122.4	0.4058	7.304
0.18	32.4	0.4145	7.461	0.70	126.0	0.3919	7.054
0.20	36.0	0.4312	7.762	0.72	129.6	0.3768	6.782
0.22	39.6	0.4457	8.023	0.74	133.2	0.3605	6.489
0.24	43.2	0.4581	8.246	0.76	136.8	0.3429	6.172
0.26	46.8	0.4687	8.437	0.78	140.4	0.3239	5.830
0.28	50.4	0.4775	8.595	0.80	144.0	0.3036	5.465
0.30	54.0	0.4848	8.726	0.82	147.6	0.2817	5.071
0.32	57.6	0.4905	8.829	0.84	151.2	0.2582	4.648
0.34	61.2	0.4947	8.905	0.86	154.8	0.2330	4.194
0.36	64.8	0.4977	8.959	0.88	158.4	0.2060	3.708
0.38	68.4	0.4994	8.989	0.90	162.0	0.1771	3.188
0.40	72.0	0.5000	9.000	0.92	165.6	0.1461	2.630
0.42	75.6	0.4995	8.991	0.94	169.2	0.1131	2.036
0.44	79.2	0.4979	8.962	0.96	172.8	0.0778	1.400
0.46	82.8	0.4953	8.915	0.98	176.4	0.0401	0.722
0.48	86.4	0.4917	8.851	1.00	180.0	0.0000	0.000
0.50	90.0	0.4878	8.780				

Model 4198

Serial 40050060-100

Formula:

$$y^2 = a_1 x + a_2 x^2 + a_3 x^3 + a_4 x^4 + a_5 x^5 + a_6 x^6$$

where $a_1 = 1.000000$

$a_2 = +1.137153$

$a_3 = -10.774885$

$a_4 = +19.784286$

$a_5 = -16.792534$

$a_6 = +5.645977$

Wetted Surface Coefficient = 0.7303

LCB, $\bar{x} = 0.4456$

Model Particulars:

Length, ft	= 15.0000
Diameter, ft	= 1.5000
Nose radius, ft	= 0.0750
Tail radius, ft	= 0.0000
Wetted surface, ft^2	= 51.622
Volume, ft^3	= 15.9043
LCB, ft	= 6.6840

REFERENCES

1. Tsakonas, Stavros, "Analytical Expressions for Thrust Deduction and Wake Fraction for Potential Flows," Stevens Institute of Technology, Experimental Towing Tank Report 717 (1957).

2. Yeh, G.C. and Martinek, J., "Interaction Force Between a Prolate Spheroid and an Axially Symmetric Vortex Ring in Potential Flow," Reed Research Inc. Final Report, Contract NOnr-2740(00), Project RR-1476 (Sep 1959).

3. Beveridge, John L., "Thrust Deduction Due to a Propeller Behind a Hydrofoil," David Taylor Model Basin Report 1603 (Oct 1962).

4. Amtsberg, H., "Untersuchungen un Rotationskörpern Über die Wechselwirkung Zuischen Schiffskörper und Propeller," Jahrbuch der Schiffbautechnischen Gessellschaft, Vol. 54 (1960).

5. Dreger, Wolfgang, "Ein Verfahren Zur Berechnung des Potentialsogs," Schiffstechnik, Vol. 6 No. 34, p. 175 (Nov 1959).

6. Korvin-Kroukovsky, B.V., "Stern Propeller Interaction with a Streamline Body of Revolution," International Shipbuilding Progress, Vol. 3, No. 17 (Jan 1956).

7. Beveridge, John L., "Effect of Axial Position of Propeller on the Propulsion Characteristics of a Submerged Body of Revolution," David Taylor Model Basin Report 1456 (Mar 1963).

8. Landweber, L. and Gertler, M., "Mathematical Formulation of Bodies of Revolution," David Taylor Model Basin Report 719 (Sep 1950).

9. Küchemann, D. and Weber, J., "Aerodynamics of Propulsion," McGraw-Hill Book Co. (1953).

10. Kaplan, C., "On a New Method for Calculating the Potential Flow Past a Body of Revolution," National Advisory Committee for Aeronautics Report 752 (1943).

11. Young, A.D. and Owen, P.R., "A Simplified Theory for Streamline Bodies of Revolution, and its Application to the Development of High-Speed Low-Drag Shapes," British R&M No. 2071 (Jul 1943).

12. Vandrey, F., "A Direct Iteration Method for the Calculation of the Velocity Distribution of Bodies of Revolution and Symmetrical Profiles," British Admiralty Research Laboratory Report ARL RI/G/HY/12/2.

13. Landweber, L., "The Axially Symmetric Potential Flow about Elongated Bodies of Revolution," David Taylor Model Basin Report 761 (Aug 1951).

14. Smith, A.M.O. and Pierce, J., "Exact Solution of the Neumann Problem. Calculation of Noncirculatory Plane and Axially Symmetric Flows About or Within Arbitrary Boundaries," Douglas Aircraft Co. Report ES-26988 (Apr 1958).

15. Granville, P., "A Method for the Calculation of the Turbulent Boundary Layer in a Pressure Gradient," David Taylor Model Basin Report 752 (1951).

16. Granville, P.S., "The Calculation of the Viscous Drag of Bodies of Revolution," David Taylor Model Basin Report 849 (1953).

17. Freeman, Hugh B., "Pressure-Distribution Measurements on the Hull and Fins of a 1/40-Scale Model of the U. S. Airship AKRON," National Advisory Committee for Aeronautics Report 443 (1932).

18. Goldstein, S., "Modern Developments in Fluid Dynamics," Vol. 2, p. 524, New York Dover Publications, Inc. (1965).

INITIAL DISTRIBUTION

Copies	
9	CHBUSHIPS 3 Tech Lib (Code 210L) 1 Lab Mgt (Code 320) 2 Prelim Des Br (Code 420) 1 Mach, Sci, & Res Sec (Code 436) 1 Submarine Br (Code 525) 1 Prop, Shaft, & Bear Br (Code 644)
1	CNO
4	CHBUWEPS 2 Tech Lib (DL 1-3) 1 Fluid Mech & Flight Sec (RRRE-4) 1 Supporting Res Br
5	CHONR 2 Fluid Dyn Br (Code 438) 1 Struc Mech Br (Code 439) 2 Undersea Programs (Code 466)
1	CDR, USNOL
1	DIR, USNRL
1	CO & DIR, USNMEL
1	CDR, USNOTS, Pasadena
1	DTMB High-Speed Phenomena Div Langley Field
1	SUPT USNAVPGSCOL
1	NAVSHIPYD PTSMH
1	NAVSHIPYD MARE
1	O in C, USN Sub School Attn: Sub Dept
1	O in C, PGSCOL, Webb
1	DIR, Aero Res, NASA
20	CDR, DDC
1	DIR DEF R&E
1	Hydro Lab, CIT
2	Dept NAME, MIT
1	DIR, St Anthony Falls Hydrau Lab

Copies	
1	DIR, ORL Attn: Dr. G.F. Wislicenus
1	DIR, DL, SIT
2	Iowa Inst of Hydrau Res, State Univ of Iowa 1 Dr. Hunter Rouse 1 Dr. L. Landweber
2	Dept NAME, Univ of Michigan Attn: Prof. R.B. Couch
1	Univ of Notre Dame Attn: Dr. A.G. Strandhagen
3	School of Engin, Univ of California 1 Prof. H.A. Schade 1 Dept of Naval Arch 1 Engr Libr
1	Oceanics, Inc. Attn: Dr. Paul Kaplan, Pres.
1	TRG
1	Hydronautics, Inc.
1	Ingalls Shipbldg Corp
1	New York Shipbldg Corp
2	Gen Dyn Corp., EB Div
1	Bethlehem Steel Co., Shipbldg Div., Quincy Attn: Mr. Hollinshead DeLuce
2	Gibbs & Cox, Inc.
1	NNSB & DD Co., Engin Tech Div Attn: Mr. John Kane
1	SNAME Attn: Captain W.N. Landers
1	Douglas Aircraft Co., Inc., Aircraft Div Long Beach Attn: Mr. A.M.O. Smith
1	CO, USNUOS
1	Naval War College, Newport (Inst of Naval Studies)
1	CO & DIR, USNMDL

Copies

1 ONR, Branch Office, Pasadena

1 Committee on Undersea Warfare

1 National Bureau of Standards
(Fluid Mechanics Section,
Dr. G. Schubauer)

1 Convair Hydrodynamics Lab, San Diego

1 Cornell Aeronautical Lab, Inc., Buffalo

1 ERG, New York

1 Grumman Aircraft Eng Corp, Bethpage
(Library)

1 Operations Research Inc., Los Angeles

1 Vidya, Inc.

UNCLASSIFIED

Security Classification

DOCUMENT CONTROL DATA ; R&D

(Security classification of title, body of abstract and indexing annotation must be entered when the overall report is classified)

1 ORIGINATING ACTIVITY *(Corporate author)* David Taylor Model Basin Washington, D.C.	2a REPORT SECURITY CLASSIFICATION UNCLASSIFIED 2b GROUP

3 REPORT TITLE

PRESSURE DISTRIBUTION ON TOWED AND PROPELLED STREAMLINE BODIES OF REVOLUTION AT DEEP SUBMERGENCE

4. DESCRIPTIVE NOTES *(Type of report and inclusive dates)*

Formal Research and Development Report

5 AUTHOR(S) *(Last name, first name, initial)*

Beveridge, John L.

6. REPORT DATE	7a TOTAL NO OF PAGES	7b. NO OF REFS
Jun 1966	30	18

8a. CONTRACT OR GRANT NO.	9a ORIGINATOR'S REPORT NUMBER(S)
b. PROJECT NO. S-R009 01 01	1665
c Task No. 0101	9b. OTHER REPORT NO(S) *(Any other numbers that may be assigned this report)*
d. Problem No. 526-083	

10 AVAILABILITY/LIMITATION NOTICES

Distribution of this document is unlimited.

11. SUPPLEMENTARY NOTES	12 SPONSORING MILITARY ACTIVITY
	Bureau of Ships Washington, D.C.

13 ABSTRACT

Measured and computed pressure distributions were obtained for a well-streamlined body of revolution (fineness ratio of ten to one), with and without a propeller, at deep submergence. Velocity distributions over the surface of the body with and without an added boundary-layer displacement-thickness are obtained from the velocity-potential function for a surface distribution of sources. Propeller-induced velocities in the near field ahead of a propeller are estimated from a uniform sink-disk representation and a single sink representation is used for large distances from the propeller. Propeller interference (image) effects are obtained from discrete singularities placed along the body axis. Within the field of propeller influence, differences occur in the theoretical and experimental pressure distributions. These discrepancies are discussed.

DD FORM 1 JAN 64 1473

UNCLASSIFIED

Security Classification

14. KEY WORDS	LINK A		LINK B		LINK C	
	ROLE	WT	ROLE	WT	ROLE	WT
Streamline Body						
Submerged						
Sources and Sinks						
Boundary Layer						
Towed						
Propelled						
Pressure Distributions on Afterbody						
Experimental						
Computed						
Propeller						
Mathematical Models (Sinks)						
Induced Velocity						
Body Interaction						

INSTRUCTIONS

1. ORIGINATING ACTIVITY: Enter the name and address of the contractor, subcontractor, grantee, Department of Defense activity or other organization *(corporate author)* issuing the report.

2a. REPORT SECURITY CLASSIFICATION: Enter the overall security classification of the report. Indicate whether "Restricted Data" is included. Marking is to be in accordance with appropriate security regulations.

2b. GROUP: Automatic downgrading is specified in DoD Directive 5200.10 and Armed Forces Industrial Manual. Enter the group number. Also, when applicable, show that optional markings have been used for Group 3 and Group 4 as authorized.

3. REPORT TITLE: Enter the complete report title in all capital letters. Titles in all cases should be unclassified. If a meaningful title cannot be selected without classification, show title classification in all capitals in parenthesis immediately following the title.

4. DESCRIPTIVE NOTES: If appropriate, enter the type of report, e.g., interim, progress, summary, annual, or final. Give the inclusive dates when a specific reporting period is covered.

5. AUTHOR(S): Enter the name(s) of author(s) as shown on or in the report. Enter last name, first name, middle initial. If military, show rank and branch of service. The name of the principal author is an absolute minimum requirement.

6. REPORT DATE: Enter the date of the report as day, month, year; or month, year. If more than one date appears on the report, use date of publication.

7a. TOTAL NUMBER OF PAGES: The total page count should follow normal pagination procedures, i.e., enter the number of pages containing information.

7b. NUMBER OF REFERENCES: Enter the total number of references cited in the report.

8a. CONTRACT OR GRANT NUMBER: If appropriate, enter the applicable number of the contract or grant under which the report was written.

8b, 8c, & 8d. PROJECT NUMBER: Enter the appropriate military department identification, such as project number, subproject number, system numbers, task number, etc.

9a. ORIGINATOR'S REPORT NUMBER(S): Enter the official report number by which the document will be identified and controlled by the originating activity. This number must be unique to this report.

9b. OTHER REPORT NUMBER(S): If the report has been assigned any other report numbers *(either by the originator or by the sponsor)*, also enter this number(s).

10. AVAILABILITY/LIMITATION NOTICES: Enter any limitations on further dissemination of the report, other than those imposed by security classification, using standard statements such as:

(1) "Qualified requesters may obtain copies of this report from DDC."

(2) "Foreign announcement and dissemination of this report by DDC is not authorized."

(3) "U. S. Government agencies may obtain copies of this report directly from DDC. Other qualified DDC users shall request through _____."

(4) "U. S. military agencies may obtain copies of this report directly from DDC. Other qualified users shall request through _____."

(5) "All distribution of this report is controlled. Qualified DDC users shall request through _____."

If the report has been furnished to the Office of Technical Services, Department of Commerce, for sale to the public, indicate this fact and enter the price, if known.

11. SUPPLEMENTARY NOTES: Use for additional explanatory notes.

12. SPONSORING MILITARY ACTIVITY: Enter the name of the departmental project office or laboratory sponsoring *(paying for)* the research and development. Include address.

13. ABSTRACT: Enter an abstract giving a brief and factual summary of the document indicative of the report, even though it may also appear elsewhere in the body of the technical report. If additional space is required, a continuation sheet shall be attached.

It is highly desirable that the abstract of classified reports be unclassified. Each paragraph of the abstract shall end with an indication of the military security classification of the information in the paragraph, represented as *(TS), (S), (C), or (U)*

There is no limitation on the length of the abstract. However, the suggested length is from 150 to 225 words.

14. KEY WORDS: Key words are technically meaningful terms or short phrases that characterize a report and may be used as index entries for cataloging the report. Key words must be selected so that no security classification is required. Identifiers, such as equipment model designation, trade name, military project code name, geographic location, may be used as key words but will be followed by an indication of technical context. The assignment of links, roles, and weights is optional.